

A novel observation of controlled carrier hopping process in B-doped Si nanocrystal/SiC multilayers at low temperatures

Yuhao Wang(王宇皓), Teng Sun(孙腾), Junnan Han(韩俊楠), Jiaming Chen(陈佳明), Ting Zhu(朱挺), Wei Li(李伟), Jun Xu(徐骏), and Kunji Chen(陈坤基)

Citation: Chin. Phys. B, 2026, 35 (**3**): 036105. DOI: 10.1088/1674-1056/adf5a6
http://cpb.iphy.ac.cn; http://iopscience.iop.org/cpb

What follows is a list of articles you may be interested in

Sensitivity investigation of 100-MeV proton irradiation to SiGe HBT single event effect

Ya-Hui Feng(冯亚辉), Hong-Xia Guo(郭红霞), Yi-Wei Liu(刘益维), Xiao-Ping Ouyang(欧阳晓平), Jin-Xin Zhang(张晋新), Wu-Ying Ma(马武英), Feng-Qi Zhang(张凤祁), Ru-Xue Bai(白如雪), Xiao-Hua Ma(马晓华), and Yue Hao(郝跃)

Chin. Phys. B, 2024, 33 (**1**): 016104. DOI: 10.1088/1674-1056/acf303

Direct observation of the distribution of impurity in phosphorous/boron co-doped Si nanocrystals

Dongke Li(李东珂), Junnan Han(韩俊楠), Teng Sun(孙腾), Jiaming Chen(陈佳明), Etienne Talbot, Rémi Demoulin, Wanghua Chen(陈王华), Xiaodong Pi(皮孝东), Jun Xu(徐骏), and Kunji Chen(陈坤基)

Chin. Phys. B, 2023, 32 (**12**): 126102. DOI: 10.1088/1674-1056/acd7cf

Sensitivity study of the SiGe heterojunction bipolar transistor single event effect based on pulsed laser and technology computer-aided design simulation

Ya-Hui Feng(冯亚辉), Hong-Xia Guo(郭红霞), Xiao-Yu Pan(潘霄宇), Jin-Xin Zhang(张晋新),Xiang-Li Zhong(钟向丽), Hong Zhang(张鸿), An-An Ju(琚安安),Ye Liu(刘晔), and Xiao-Ping Ouyang(欧阳晓平)

Chin. Phys. B, 2023, 32 (**6**): 066105. DOI: 10.1088/1674-1056/ac8f3b

A new direct band gap silicon allotrope *o*-Si32

Xin-Chao Yang(杨鑫超), Qun Wei(魏群), Mei-Guang Zhang(张美光), Ming-Wei Hu(胡明玮), Lin-Qian Li(李林茜), and Xuan-Min Zhu(朱轩民)

Chin. Phys. B, 2022, 31 (**2**): 026104. DOI: 10.1088/1674-1056/ac11db

Quantum confinement and surface chemistry of 0.8-1.6 nm hydrosilylated silicon nanocrystals

Pi Xiao-Dong (皮孝东), Wang Rong (王蓉), Yang De-Ren (杨德仁)

Chin. Phys. B, 2014, 23 (**7**): 076102. DOI: 10.1088/1674-1056/23/7/076102

A novel observation of controlled carrier hopping process in B-doped Si nanocrystal/SiC multilayers at low temperatures

Yuhao Wang(王宇皓)[1], Teng Sun(孙腾)[1], Junnan Han(韩俊楠)[1], Jiaming Chen(陈佳明)[1], Ting Zhu(朱挺)[2], Wei Li(李伟)[1], Jun Xu(徐骏)[1,2,†], and Kunji Chen(陈坤基)[1]

[1] *National Laboratory of Solid State Microstructures, State Key Laboratory of Spintronics, School of Electronics Science and Engineering, Collaborative Innovation Center of Advanced Microstructures, Jiangsu Provincial Key Laboratory of Advanced Photonic and Electrical Materials, Nanjing University, Nanjing* 210000, *China*

[2] *School of Microelectronics and School of Integrated Circuits, Jiangsu Key Laboratory of Semi. Dev. & IC Design, Package and Test, Nantong University, Nantong* 226019, *China*

(Received 9 June 2025; revised manuscript received 17 July 2025; accepted manuscript online 30 July 2025)

Recent advances in quantum computing devices make studies on the carrier transport behaviors of silicon nanocrystals (Si NCs) under cryogenic temperature a most important subject. In this work, we study the electrical properties modified by B dopants in Si NC/SiC multilayers. Mobility measurement shows that the scattering mechanism that dominates in our samples in a low temperature range is ionized impurity scattering. Three carrier transport behaviors are identified as variable range hopping (VRH) (20–100 K), multiple phonon hopping (MPH) (100–500 K) and thermally-activated mechanisms (500–660 K). At temperature ranges as low as 30 K, we observe the effect of the Coulomb gap in B-doped Si NC/SiC multilayers that obey the Efros and Shklovskii (ES) law, which was not present in our previous studies concerning Si NC multilayers. The crossover temperature T_C is observed to increase with rising B-doping concentrations, which demonstrates another interesting effect of doping in controlling the electrical properties of Si NCs.

Keywords: Si NCs, B dopants, Hall mobility, variable range hopping

PACS: 61.72.uf, 61.82.Rx, 61.72.U–, 73.20.Fz

DOI: 10.1088/1674-1056/adf5a6 **CSTR:** 32038.14.CPB.adf5a6

1. Introduction

Since the discovery of the size-dependent bandgap and quasi-direct band structure of silicon nanocrystals (Si NCs) under the quantum confinement effect, Si NC-based devices have been extensively studied and applied in the areas of optoelectronics, synaptic devices and telecommunication.[1–3] Recent advances in Si-based quantum processing devices indicate that comprehensively understanding the electrical properties of Si NCs at cryogenic temperatures is of great importance for promoting quantum processing.[4–7] It is also found in quantum computing that when subjected to a transverse magnetic field, a heavy-hole state can effectively decouple the hole spin from nuclear spins. This suppression of nuclear spin effects leads to longer coherence times for hole spins, which demonstrates the importance of studies on the B-doping mechanism in Si NCs.[8] Doping in Si NCs directly affects their grain size and defect states, making doping behavior studies much more complicated than bulk Si. This observation, together with the increasing demand for high-performance Si-based electronic devices, makes studying the low temperature characteristics of doped Si NCs very promising research.

In our previous work, we have investigated the doping behaviors of P and B in Si NCs and found that dopants can not only provide free carriers but also passivate the dangling bonds, promoting the electronic properties and structure of Si NCs.[9–12] Specifically, our group has studied the effect of B-dopants in Si NC/SiO_2 multilayers, and discussed their carrier transport mechanisms. Notably, recent studies have reported that SiC can be chosen as a dielectric layer for its lower bandgap compared to SiO_2, which is beneficial in terms of better carrier injection and superior device performance.[13–15] It has also been found that P dopants can induce Si vacancies within Si NC/SiC multilayer systems, which may benefit Si-based quantum computing devices.[16] In this work, size-controlled ($\sim$ 13 nm) B-doped Si NC multilayer samples with SiC dielectric layers are fabricated by a plasma enhanced chemical vapor deposition (PECVD) system. Electrical properties of B-doped Si NC/SiC multilayers, especially under low temperature, are studied by Hall effect measurements. Ionized impurity scattering is proved to be the main scattering mechanism in our samples. Variable temperature conductivity measurements yielded mainly three carrier transport behaviors that dominated different temperature ranges: variable range hopping (VRH) (20–100 K), multiple phonon hopping (MPH) (100–500 K) and thermally-activated mechanisms (500–660 K). It is observed that at temperature under 30 K, carriers obey the Efros–Shklovskii (ES) law, which arises when the Coulomb interaction cannot be neglected. Notably, this crossover temperature (T_C) increases with the ris-

†Corresponding author. E-mail: xjun@ntu.edu.cn, junxu@nju.edu.cn

© 2026 Chinese Physical Society and IOP Publishing Ltd. All rights, including for text and data mining, AI training, and similar technologies, are reserved.

ing doping concentration, which demonstrates the remarkable effect of doping in our sample. We have illustrated the hopping behavior of carriers in B-doped Si NC/SiC multilayers at low temperature and provided a viable solution to control their crossover behavior. As such, this could promote research in areas such as quantum computing and deep space exploration which are carried out at low temperature.[17,18]

2. Experiment

B-doped amorphous Si (a-Si)/SiC multilayers were first fabricated on Si (100) wafers and quartz substrates by a PECVD system with a radio frequency of 13.56 MHz. The deposition chamber was evacuated to a pre-vacuum pressure below 10^{-4} Pa using a barometer, and the substrate surfaces were further cleaned with H_2 plasma. A gas mixture of SiH_4 and B_2H_6 gas (2%, H_2 dilution) was then introduced into the chamber and ionized to deposit the B-doped Si sublayers. During the deposition process of the Si sublayer, the gas flow rate of SiH_4 was kept at 10 sccm, while the B_2H_6 gas varied from 0, 3 sccm, 5 sccm, 15 sccm and 20 sccm. The elemental ratio calculated by the gas flow ratio of B_2H_6/SiH_4 was defined as the nominal doping ratio of the B-doped sample. The gas mixtures of SiH_4 (5 sccm) and CH_4 (50 sccm) were used to deposit the SiC sublayers. After the deposition of one specific layer, the chamber was evacuated to below 1 Pa before introducing the next layer's gas mixture. The a-Si sublayer and SiC sublayer were deposited alternately to form a-Si and SiC stacked multilayers of nine cycles. During the whole deposition process, the RF power and chamber temperature were kept at 5 W and 250 °C, respectively. The as-deposited multilayer samples were subsequently dehydrogenated at 450 °C and then annealed at 1000 °C for 1 h under ambient N_2. Al electrodes were deposited at the surface of the quartz sample for Hall characterization by magnetron sputtering; the electrodes were designed to be 1×1 mm at the four corners, according to van der Pauw (VDP) geometry.

The microstructures of Si NC/SiC multilayers were characterized by transmission electron microscopy (TEM, TECNAI G^2F20 FEI). The crystalline characteristic was measured by Raman scattering spectra (Horiba Scientific LabRAM HR Evolution, 514 nm laser). The electrical properties were studied by Hall effect measurements (LakeShore 8400 series) based on VDP geometry.

3. Results and discussion

Figures 1(a) and 1(b) show the cross-sectional TEM image of the B-doped Si NC/SiC multilayers, with the layer boundaries clearly visible. The Si and SiC layers are estimated to be 13 nm and 8 nm thick, and individual Si NCs can be identified within the Si NC layers. A broad Raman envelope near 480 cm^{-1} can be measured in the unannealed sample featured in Fig. S1, which is related to the transverse optical (TO) mode of the amorphous Si–Si bond.[19,20] Furthermore, an asymmetric Raman peak around 511 cm^{-1} is observed for all B-doped samples after annealing in Fig. 1(c), which corresponds to the TO mode of crystallized Si phases. The Raman peaks red shift slightly with the increase of the doping concentration, which can be explained by the tensile stress induced by the B atoms with significantly smaller atom radius than Si.[21] These results are consistent with the TEM images, which show that the a-Si sublayers crystallize to form Si NCs after high-temperature annealing.

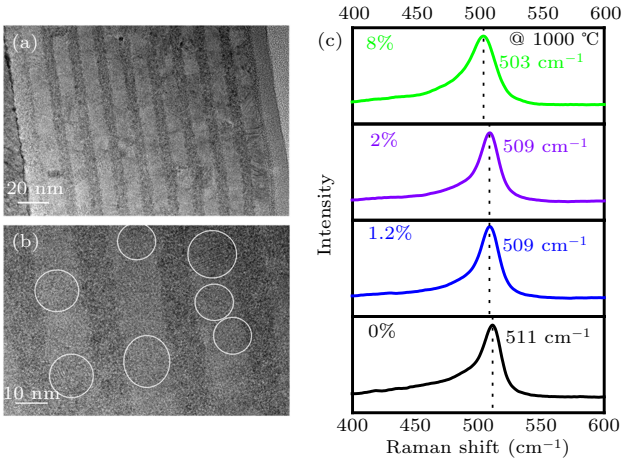


Fig. 1. Schematic of the cross-sectional TEM image of the Si NC/SiC multilayer sample in (a) 20 nm scale and (b) 10 nm scale. (c) Raman spectrum of 1000 °C annealed Si NC/SiC multilayers under different doping concentrations.

The effect of B-doping on the electrical properties of Si NC/SiC multilayers has been investigated using Hall effect measurements. Figure 2(a) illustrates the room temperature carrier concentration of Si NC/SiC multilayers with varying B-doping levels. For the undoped Si NC/SiC multilayers, the carrier concentration is approximately 7.01×10^{15} cm^{-3}. Upon introducing the B dopants, the carrier concentration increases rapidly by four orders of magnitude, reaching around 5.93×10^{19} cm^{-3}. This significant increase in carrier concentration suggests that a large number of B dopants have substituted into the Si lattice sites and become electrically activated. As depicted in Fig. 2(b), the carrier mobility is also influenced by the B-doping ratios, initially increasing and then gradually decreasing. In our previous research, we found that doping can improve carrier mobility in Si NCs by reducing the barrier height at grain boundaries and lowering surface defect states, thus weakening the scattering effect of grain boundaries. However, excessive doping can damage the Si crystalline lattice and create additional ionized impurity centers. These defects, resulting from lattice damage, often act as traps for carriers, leading to a decrease in mobility.[22] Furthermore, the increased collision scattering between carriers and the activated B dopants in lattice sites may also contribute to the reduction in carrier mobility. Figure S2 displays the carrier con-

centration and mobility with changing temperature and doping ratio. For the carrier concentration, it increases with the rising temperature, while the carrier mobility first rises then begins to decline under high temperature. The tendency to decline can be explained by the enhanced lattice vibration scattering induced by high temperature.

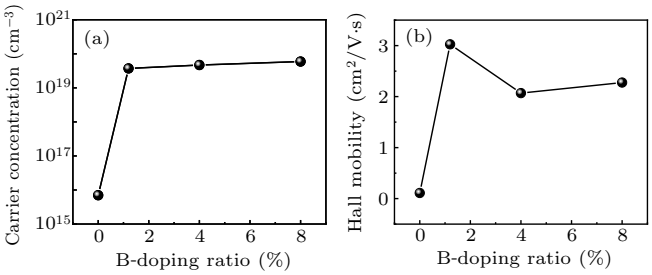


Fig. 2. Room temperature (a) carrier concentration and (b) Hall mobility of Si NC/SiC multilayers with various B-doping ratios.

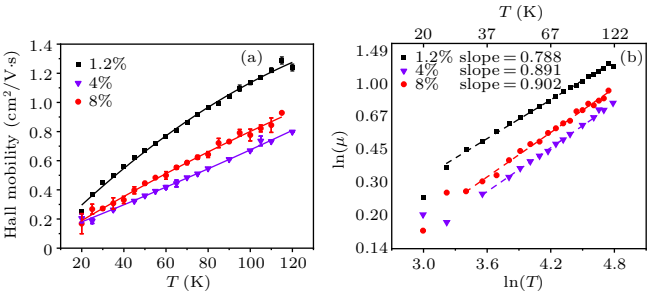


Fig. 3. (a) Variable temperature Hall mobility between 20–100 K. (b) Variable temperature Hall mobility plotted against temperature on a log–log scale.

To further study the carrier scattering mechanism at low temperatures, we tested the Hall mobility between 20 K and 100 K. The results are plotted in Fig. 3(a), where carrier mobility increases with temperature but decreases as the doping concentration rises. The effect of lattice vibration scattering and ionized impurity scattering on the carrier mobility in this temperature range is studied by further plotting the logarithm of mobility against the logarithm of temperature to determine the dominant scattering mechanism. The dashed line in Fig. 3(b) is the linear fit of the plotted results. It can be observed that the carrier mobility temperature dependence obeys the following equation:

$$\mu_{\mathrm{H}}(T) \propto T^{n}. \tag{1}$$

For c-Si, the values of n for lattice vibration scattering, ionized impurity scattering, and neutral impurity scattering are -1.5, 1.5, and 0, respectively. Figure 3(b) indicates that the exponential values of n calculated from the fitted slope are 0.788, 0.891, and 0.902 for 1.2%, 4%, and 8% B-doped samples, respectively. The increase in the n value close to 1.5 with rising doping concentration not only demonstrates the stronger dominance of ionized impurity scattering induced by higher doping concentrations, but also shows that the main scattering mechanism that affects carrier mobility under this varying temperature range is ionized impurity scattering.

Variable temperature conductivity characteristics are also analyzed to provide further knowledge about carrier transport mechanisms. Figure 4 shows the conductivity of B-doped Si NC/SiC multilayers against temperature. The solid and dashed lines stand for the fitted curve and linear fitting of our results, respectively. In Fig. 4(a), we observe that at temperatures above 500 K, the thermally-activated conduction mechanism dominates, which is depicted by the following Arrhenius relationship:

$$\sigma = \sigma_0 \exp\left(-\frac{E_{\mathrm{a}}}{k_0 T}\right), \tag{2}$$

where E_{a} is the conductivity activation energy and k_0 stands for the Boltzmann constant.[9,19,23] This agreement shows that its carrier transport mechanism above 500 K follows the thermally-activated conduction mechanism. For B-doped P-type semiconductors, E_{a} represents the difference between the Fermi energy E_{F} and the valance band maximum E_{v} — the value of which can be derived from the slope of the ln σ–T^{-1} plot as 51 meV, 56.7 meV and 53 meV for the 1.2%, 4% and 8% B-doped samples, respectively. The E_{a} of the un-doped Si NC samples is 499.4 meV; this comparison shows that the Fermi energy is very close to the valance band maximum after effective B doping.[9] Lowering the temperature to about 100 K, we find that the conductivity and T^{y} plotted on the log–log scale in Fig. 4(b) exhibit a linear relationship. This indicates at this temperature range, electron transport follows a MPH mechanism, as is shown below:

$$\sigma \propto T^{y}, \tag{3}$$

where y is the ratio of the average site energy difference to the average energy of phonon modes coupled to the electrons.[9,24,25] Under the MPH process, the carriers are weakly localized and are easy to couple with phonons with wavelengths close to their localization length. In our previous works, we found that with the increase of the P-doping concentration in the Si NC/SiC multilayers, the temperature at which the carrier transport mechanism shifts from MPH to thermally-activated lowers, whereas in our case it stays the same.[9] We believe that this is because B has a much smaller atom radius than Si which makes it harder to incorporate into the Si NCs. When we further decrease the temperature, the Mott-VRH mechanism begins to dominate as is plotted in Fig. 4(c) according to the following formula:

$$\sigma \propto \exp\left[-\left(\frac{T_{\mathrm{M}}}{T}\right)^{\frac{1}{4}}\right], \tag{4}$$

where T_{M} is the Mott parameter.[26] When the temperature is reduced to lower than the freeze-out limit of acoustic phonons, and carrier transport is dominated by carriers which tunnel from occupied localized sites to unoccupied localized sites,[27]

in the transition from VRH and MPH to thermally-activated conduction mechanisms, a change from hopping-dominated insulator behavior to a metallic conduction mechanism occurs. This suggests that our sample may exhibit metal–insulator transition under low temperature due to the Anderson localization of impurities and defects, which localizes the wave function of carriers to impede carrier transport. According to previous research, both increasing temperature and doping concentrations contribute to the higher localization length of carriers. In addition, when the carrier localization length significantly exceeds the particle scale, the electrons become delocalized and become free carriers.[28]

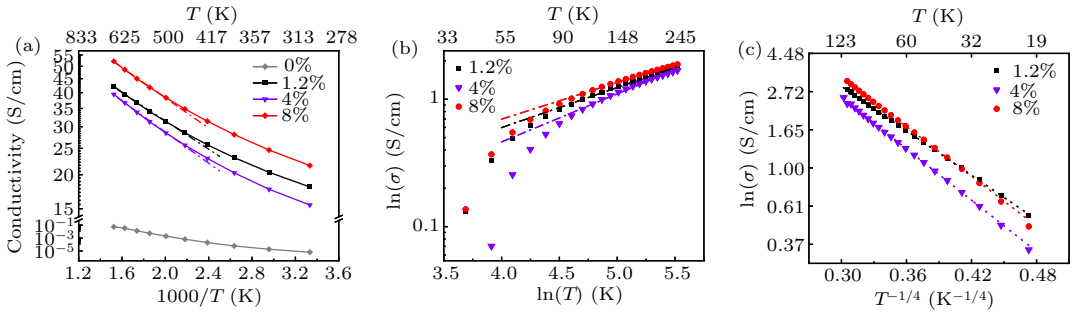


Fig. 4. Fitted diagrams of (a) conductivity of Si NC/SiC multilayers under thermally-activated transport mechanisms above 500 K. (b) MPH process at temperature ranges above 100 K. (c) Mott-VRH mechanism below 100 K.

Interestingly, a deviation in the fitted plot of Fig. 4(c) occurs below 30 K, which illustrates a transition to another law. To analyze this phenomenon, we plotted $\ln\sigma$ against $T^{-1/2}$ and $T^{-1/4}$ with the ES-VRH relationship given as follows:

$$\sigma \propto \exp\left[-\left(\frac{T_{\mathrm{ES}}}{T}\right)^{\frac{1}{2}}\right], \tag{5}$$

where T_{ES} is the ES parameter.[29] The results are shown in Fig. 5(a) where a linear relation presented by the dashed line is clearly observed for ES-VRH below 40 K. The transition temperature T_{C} from ES to Mott-VRH appears to rise with increasing doping concentration. To verify our observation, the transition temperature T_{C} can be derived from T_{ES} and T_{M} by the following formula:[29,30]

$$T_{\mathrm{C}} = 16\frac{T_{\mathrm{ES}}^2}{T_{\mathrm{M}}}. \tag{6}$$

The T_{ES} and T_{M} can be calculated by the slope of the fitted curves in Figs. 5(a) and 5(b), and the T_{C} is calculated to be 22.25 K, 26.65 K and 35.66 K for the 1.2%, 4% and 8% B-doped samples. The observed temperature range where ES-VRH dominates, as shown by the fitted curve, is slightly larger than the calculated T_{C} figure. This is due to the crossover from ES to Mott-VRH being a smooth transition where the exponent changes from $-1/2$ to $-1/4$. The crucial observation that makes our perspective credible is the tendency of T_{C} to increase which matches the calculated T_{C} by the fitted T_{ES} and T_{M}. The increase of T_{C} can be explained by the fact that a higher doping concentration increases the density of state at the Fermi level.[30] The relationship between T_{C} and $N(E_{\mathrm{F}})$ is as follows:

$$T_{\mathrm{C}} = \frac{e^4 a N(E_{\mathrm{F}})}{k_{\mathrm{B}}(4\pi\varepsilon\varepsilon_0)^2}, \tag{7}$$

where $N(E_{\mathrm{F}})$ is the density of state at the Fermi energy level.[31] When the temperature is lowered below T_{C}, the Coulomb interaction cannot be neglected and reduces the density of state at the Fermi level; this causes the transition from Mott to ES laws. In addition, when the localization length ξ is larger than the size of the NCs, the Mott-VRH prefers to replace the ES-VRH to dominate the carrier transport due to the reduced Coulomb effect.[9] Therefore, in systems that have high orders of disorder which result in small localization length, ES-VRH is easier to replace Mott-VRH which increases the T_{C}. Higher doping concentrations also induce greater fluctuations in in doners per NC, which enhances the Coulomb gap within our samples. These factors all contribute to the increase of T_{C} with doping concentrations in our samples.[32] T_{C} in usual amorphous materials is extremely low; in amorphous Ge the number of which is 0.15 K.[31] In crystalline materials such as Si, the low level of disorder results in a very low crossover temperature of 1 K,[33] whereas in porous Si, the T_{C} is significantly higher, reaching 120 K.[34] In NC systems, the quantum confinement effect induces discrete energy levels and increases the density of state at the Fermi level. Si NCs and CdSe NCs have been reported to have a T_{C} of 160 and 120 K, while research on discontinuous silver reveals an even higher T_{C} at 250 K.[31,35,36] The moderate T_{C} of our sample around 30 K ensures the stability of carrier transport behaviors at low temperature, while it maintains a fairly good electrical property compared to higher disordered systems. Further, our observation of T_{C} with varying B-doping concentrations demonstrates the potential of doping in manipulating the electrical properties of Si NCs even at low temperatures. The tunable crossover temperature also demonstrates that in our NC sample, the Coulomb gap plays a very important role and could provide valuable guidance to its de-

vice fabrication aimed at low temperature performance.

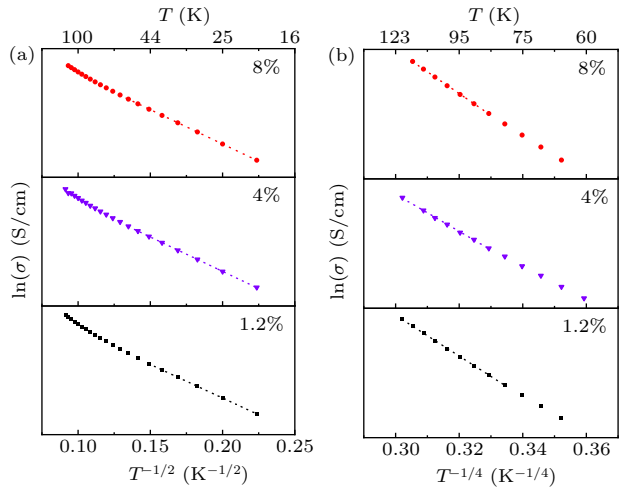


Fig. 5. Fitted diagrams of (a) ES-VRH between 20–100 K and (b) Mott-VRH between 60–120 K.

4. Conclusions

In summary, B-doped Si NC/SiC multilayers were fabricated by a PECVD system. Hall effect measurement shows that in a Si NC/SiC multilayer system, B-doping successfully induces free carriers up to four orders of magnitude. We discover that in the temperature range below 100 K, the main scattering mechanism that takes effect is ionized impurity scattering. By conductivity analysis, three main carrier transport behaviors can be identified as VRH, MPH and thermally-activated mechanisms. The carrier transport mechanism under 100 K is dominated by the VRH process, which shifts from Mott to ES-VRH when the temperature is reduced to below T_C ($\sim$ 30 K). The increase in crossover temperature with rising doping concentration demonstrates the tuning effect of B-doping within our samples. ES-VRH proves the existence of the Coulomb gap and strong Coulomb interaction effect at low temperature, and is a novel observation of such behavior in multilayer Si NC systems. The relatively high and tunable T_C observed in our sample is a notable observation, and is of great importance in terms of device applications.

Acknowledgements

This work is supported by Quantum Science and Technology – National Science and Technology Major Project (Grant No. 2024ZD0301100), the National Key R&D Program of China (Grant No. 2018YFB2200101), and the National Natural Science Foundation of China (Grant Nos. 61921005 and 62004078).

References

[1] Tan H, Ni Z, Peng W, Du S, Liu X, Zhao S, Li W, Ye Z, Xu M, Xu Y, Pi X and Yang D 2018 *Nano Energy* **52** 422
[2] Mastalieva V, Neplokh V, Aybush A, Stovpiaga E, Eurov D, Vinnichenko M, Karaulov D, Kirillenko D, Mozharov A, Sharov V, Kolchanov D, Machnev A, Golubev V, Smirnov A, Ginzburg P, Makarov S, Kurdyukov D and Mukhin I 2024 *Nanophotonics* **13** 3299
[3] Huh C, Kim T Y, Ahn C G and Kim B K 2015 *Appl. Phys. Lett.* **106** 211103
[4] Yang T Y, Ruffino A, Michniewicz J, Peng Y, Charbon E and Gonzalez-Zalba M F 2020 *IEEE Electron Device Lett.* **41** 981
[5] Ruffino A, Yang T-Y, Michniewicz J, Peng Y, Charbon E and Gonzalez-Zalba M F 2021 *Nat. Electron.* **5** 53
[6] Zhao S, Yuan G, Zhu Q, Song L, Zhang D, Liu Y, Lu J, Han W and Luo J 2022 *IEEE Trans. Electron Devices* **69** 2585
[7] Zhang Y, Lu T, Wang W, Zhang Y, Xu J, Luo C and Guo G 2021 *IEEE Trans. Electron Devices* **68** 4267
[8] Prechtel J H, Kuhlmann A V, Houel J, Ludwig A, Valentin S R, Wieck A D and Warburton R J 2016 *Nat. Mater.* **15** 981
[9] Sun T, Li D, Chen J, Han J, Li W, Xu J and Chen K 2023 *Vacuum* **207** 111657
[10] Chen J, Li D, Sun T, Han J, Zhang Y, Li W, Xu J and Chen K 2023 *Nanotechnology* **34** 16
[11] Li D, Han J, Sun T, Chen J, Talbot E, Demoulin R, Chen W, Pi X, Xu J and Chen K 2023 *Chin. Phys. B* **32** 126102
[12] Han J, Wang Y, Chen J, Sun T, Li D, Li W, Xu L, Xu J and Chen K 2025 *Opt. Lett.* **50** 3927
[13] Sun T, Wang Y, Han J, Chen J, Zhu T, Li D, Li W, Xu J and Chen K 2024 *Appl. Phys. Lett.* **125** 031105
[14] Rui Y, Li S, Cao Y, Xu J, Li W and Chen K 2013 *Appl. Surf. Sci.* **269** 37
[15] Rui Y, Li S, Xu J, Song C, Jiang X, Li W, Chen K, Wang Q and Zuo Y 2011 *J. Appl. Phys.* **110** 064322
[16] Sun T, Li D, Chen J, Han J, Zhu T, Li W, Xu J and Chen K 2023 *Appl. Surf. Sci.* **613** 155983
[17] Patterson R L, Hammoud A and Elbuluk M 2006 *Cryogenics* **46** 231
[18] Gonzalez-Zalba M F, De Franceschi S, Charbon E, Meunier T, Vinet M and Dzurak A S 2021 *Nat. Electron.* **4** 872
[19] Chen J, Li D, Zhang Y, Jiang Y, Xu J and Chen K 2020 *Appl. Surf. Sci.* **529** 146971
[20] Li D, Chen J, Sun T, Zhang Y, Xu J, Li W and Chen K 2022 *Opt. Express* **30** 12308
[21] Saleh R and Nickel N H 2007 *Appl. Surf. Sci.* **254** 580
[22] Shan D, Ji Y, Li D, Xu J, Qian M, Xu L and Chen K 2017 *Appl. Surf. Sci.* **425** 492
[23] Bronger T, Astakhov O and Carius R 2019 arXiv:1908.06516 [cond-mat.mtrl-sci]
[24] Qian M, Shan D, Ji Y, Li D, Xu J, Li W and Chen K 2016 *Nanoscale Res. Lett.* **11** 346
[25] Das D and Sain B 2013 *J. Appl. Phys.* **114** 073708
[26] Zvyagin I P, Kurova I A and Ormont N N 2004 *Phys. Status Solidi C* **1** 101
[27] Yildiz A, Serin N, Serin T and Kasap M 2009 *Jpn. J. Appl. Phys.* **48** 111203
[28] Chen T, Reich K V, Kramer N J, Fu H, Kortshagen U R and Shklovskii B I 2016 *Nat. Mater.* **15** 299
[29] Rafiq M A 2018 *J. Semicond.* **39** 061002
[30] Huang Y L, Chiu S P, Zhu Z X, Li Z Q and Lin J J 2010 *J. Appl. Phys.* **107** 063715
[31] Yu D, Wang C, Wehrenberg B L and Guyot-Sionnest P 2004 *Phys. Rev. Lett.* **92** 216802
[32] Chen T, Reich K V, Kramer N J, Fu H, Kortshagen U R and Shklovskii B I 2016 *Nat. Mater.* **15** 299
[33] Limouny L, El Kaaouachi A, Dlimi S, Sybous A, Narjis A, Errai M and Daoudi E 2013 *Mod. Phys. Lett. B* **27** 1350146
[34] Islam Md N, Ram S K and Kumar S 2009 *Physica E* **41** 1025
[35] Inada M, Yamamoto H, Gibo M, Ueda R, Umezu I, Tanaka S, Saitoh T and Sugimura A 2015 *Appl. Phys. Express* **8** 105001
[36] Mandal S K, Gangopadhyay A, Chaudhuri S and Pal A K 1999 *Vacuum* **52** 485